01 Jan 2024

Fabrication And Analysis Of A Gas Sensor Utilizing A Fabry-Perot Interferometer With Varied Thicknesses Of ZIF-8 Coating On End-Faced Single-Mode Optical Fiber

Nahideh Salehifar

Rex E. Gerald
Missouri University of Science and Technology, geraldr@mst.edu

Jie Huang
Missouri University of Science and Technology, jieh@mst.edu

Recommended Citation

N. Salehifar et al., "Fabrication And Analysis Of A Gas Sensor Utilizing A Fabry-Perot Interferometer With Varied Thicknesses Of ZIF-8 Coating On End-Faced Single-Mode Optical Fiber," *IEEE Sensors Journal*, Institute of Electrical and Electronics Engineers, Jan 2024.
The definitive version is available at https://doi.org/10.1109/JSEN.2024.3366872

This article has been accepted for publication in IEEE Sensors Journal. This is the author's version which has not been fully edited and content may change prior to final publication. Citation information: DOI 10.1109/JSEN.2024.3366872

Fabrication and Analysis of a Gas Sensor Utilizing a Fabry-Perot Interferometer with Varied Thicknesses of ZIF-8 Coating on End-Faced Single-Mode Optical Fiber

Nahideh Salehifar*, Rex E. Gerald II, and Jie Huang*, Senior Member IEEE

Abstract— This research investigates the potential of integrating optical fiber and sensitive thin film coating materials to develop diverse chemical sensing platforms. We utilized a layer-by-layer synthesis technique, along with specific pre- post treatment methods, to create highly effective nonporous metal-organic frameworks (MOFs), specifically ZIF-8, ranging from the nanometer scale to the micrometer scale (800 nm to 110 µm). Additionally, we successfully cultivated ZIF-8 on both sides of a single-mode fiber (SMF) with thicknesses of 25 µm and 50 µm.

In a separate experiment, we successfully grew ZIF-8 on one side of an optical fiber, achieving a thickness of 10 µm. The sensor demonstrated notable sensitivity to ethanol, with the fringe valley shifting from 1602 nm to 1606.8 nm as the ethanol concentration increased from 30 ppm to 70 ppm. Reducing the thickness of the MOF coating led to notable improvement in response and recovery times. Specifically, for a 10 µm cavity length, response time decreased to around 17 seconds and recovery time to 50 seconds, compared to 110 µm cavities which took 1 minute to respond and 4 minutes to recover at room temperature.

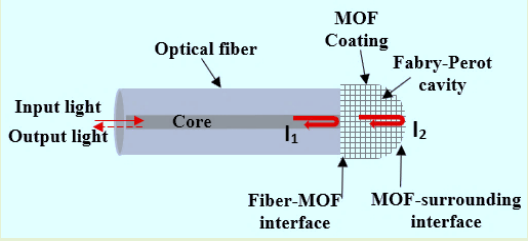

Index Terms— Metal-Organic Framework, External Fabry Perot Interferometer (EFPI), Optical Fiber, Gas sensors, Optical sensors.

I. INTRODUCTION

Gas sensors play a crucial role in a variety of applications, including the detection of hazardous gases, monitoring of indoor air quality, facilitation of industrial processes, quality control in the food industry, environmental assessments, and medical diagnostics.

This work was supported by the Army Research Laboratory and was accomplished under Cooperative Agreement Number W911NF-21-2-0274. The views and conclusions contained in this document are those of the authors and should not be interpreted as representing the official policies, either expressed or implied, of the Army Research Office or the U.S. Government.

Nahideh Salehifar is with the Department of Electrical and Computer Engineering, Missouri University of Science and Technology

Rex E. Gerald is with the Department of Electrical and Computer Engineering, Missouri University of Science and Technology, Rolla, MO 65409 USA.

Jie Huang is with the Department of Electrical and Computer Engineering, Missouri University of Science and Technology, Rolla, MO 65409 USA.

Despite the availability of a wide array of portable chemical sensors, there is a continuous demand for innovative technologies in this sector [1-7]. Gas sensors can be categorized based on their signal transduction methods, which can be electrical, optical, or acoustic [8, 9]. One such method is solvatochromism, a powerful signal transduction technique that involves monitoring color changes in a material due to the significant shifts in its absorption spectrum [10].

Another approach is luminescence sensing, using a metal-organic framework (MOF). In this method, fluorescence signals are enhanced, quenched, or altered in response to the detection of a target substance. Luminescent MOF sensors have proven successful in detecting oxygen-based explosives,

various aromatic compounds, and amines. However, their application in biological sensing has been restricted [11-14].

Alternative methods such as Interferometry [15, 16], Localized Surface Plasmon Resonance (LSRP) [17], and Colloidal Crystals [16] offer different approaches. Unlike luminescence and solvatochromism, these methods do not rely on light absorption or emission. Optical absorption spectroscopy, a technique used since the inception of optics, is employed to determine the composition of materials. Its success is closely tied to the optical thickness of the substance being analyzed, a factor that can be greatly boosted by incorporating it into an optical cavity. Optical gas sensors operate by detecting alterations in light due to their interaction with molecules which can manifest as absorption, emission, or scattering. These sensors are available in a variety of configurations, each serving distinct purposes, resulting in a broad range of classification methods. Generally, optical gas sensors can be classified into two categories: dispersive and non-dispersive [18]. Fiber optic sensors as optical gas sensors are in high demand for gas sensing across diverse applications due to their exceptional performance in challenging conditions, such as extreme temperatures and corrosive environments. Compared to metal-based systems, sensors that utilize optical fiber (OF) technology offer numerous advantages. These include resistance to electromagnetic interference, the capability for wireless operation without electricity, exceptional thermal and chemical stability, and the potential for implementing distributed sensing platforms [19-21]. There are several types of fiber optic sensors, including fiber grating sensors [22], fiber optic gyroscope sensors [23], and interferometer sensors [24], each available in various configurations.The development of coatings for optical fiber sensors is essential for enhancing the detection of target chemicals through Fabry-Perot interferometric cavities (FPI). However, over time, the properties of the coated components within the cavity may change [25].

MOFs are complex structures of metal ions and organic linkers known for their porous crystalline nature. They can be customized to capture specific gas molecules by adjusting pore sizes. The large internal surface area of MOFs enhances gas concentration, altering the refractive index noticeably. These materials are highly chemically and thermally stable due to strong metal-oxygen-carbon bonds [16, 26-28]. Previous studies have extensively explored various applications of MOFs, including selective hydrogen gas storage [29], specific gas adsorption [30], separation processes [31], and catalysis [32]. The unique capability to modify pore sizes and perform post-synthesis functionalization enables the creation of MOFs that can selectively interact with target analytes. This allows only molecules of a certain size or functional group to enter their cavities. Although the development of MOF-based sensors has been somewhat limited, early reports suggest their potential to evolve into highly effective analytical devices [33].

Researchers have effectively employed optical transduction methods in MOF sensors, which involve the use of thin MOF films on silicon or plasmonic substrates. As an example, coatings of Cu-BTC (HKUST-1) were applied to both single-mode and multimode optical fibers (OF) to detect carbon dioxide. Alternatively, an etched OF with a thin ZIF-8 layer was utilized for UV-band optical absorption spectroscopy [34-36]. In another research, UiO-66 was applied to the end-face of an OF probe to detect Rhodamine-B [37]. Efficient utilization of MOFs for chemical sensors requires effective signal transmission. Gas sensors using MOFs and refractive index (RI) as the sensing mechanism have been developed. RI-based sensing utilizes the medium's refractive index and is common in measuring various parameters across optical spectral ranges, including communications [38]. Advanced MOF technology allows RI-based gas sensing with amplified gas concentration due to the high surface area, enhancing refractive index changes from gas variations. Initiatives exist to develop RI-based gas sensors with MOFs [16, 27]. ZIF-8, a specific type of metal-organic framework (MOF), has garnered interest for its potential in sensor development, owing to its exceptional chemical durability and thermal stability, which stem from its sodalite structure [39, 40].

The kinds of literature reveal significant advancements in utilizing ZIF-8 for optical fiber-based gas sensing. Notably, Kim et al. [41] developed a CO_2-selective sensor using a 200 nm ZIF-8 thin film on an optical fiber core, exhibiting a sensitivity of 1.33 pm ppm^{-1} in the linear range from 9.8 ppm to 540 ppm for ethanol vapor. Additionally, an optical fiber long-period grating (LPG) sensor coated with ZIF-8 demonstrated a sensitivity of 0.015 ± 0.001 and 0.018 ± 0.0015 nm/ppm and a limit of detection (LOD) of 6.67 ppm and 5.56 ppm for acetone and ethanol respectively [42]. Another study proposed a RI-based fiber-optic sensor employing MOF-based dual Fabry-Perot nanocavities, achieving enhanced sensitivity (48.5 mV/CO_2 Vol%) and a resolution of 0.019 CO_2 Vol% [3]. Furthermore, an LPG modified with ZIF-8 thin film exhibited a response to organic vapors with the lowest detection of 1454 ppm.

The study emphasizes the importance of MOF selection, such as ZIF-8, for its specific adsorption capabilities, leading to high selectivity and sensitivity [26]. Rongtao et.al presented a low-cost optical fiber methane (CH_4) gas sensor, utilizing a ZIF-8 and silicone polymers based on PDMS coating, achieving a 1% detection limit in N_2. The sensor exhibits excellent CH_4 selectivity over N_2, with a principle based on refractive index shifts in the polymer layer upon methane dissolution, resulting in a highly sensitive and cost-effective detection method [43].

Huang et.al explored enhanced light-matter interaction in photonic devices by synthesizing multilayer ZIF-8 nanoparticles on a graphene oxide-premodifier optical fiber, demonstrating a fast sensor response (118 ms) with a low detection limit (5.26 ppm) for ethanol sensing at room temperature [44]. Kim et al. coated Alkylamine-modified ZIF-8 on the optical fiber sensors to improve CO_2 sensing by mitigating water interference, ensuring stability, sensitivity, and potential applications in CO_2 capture under humid conditions (FT-IR and breakthrough studies confirmed the result) with a response time of around 10–15 min [45]. However, challenges arise in all the cited research, including the impact of humidity and temperature on sensor performance. This necessitates the utilization of extra

polymers, metals, or a modification process involving MOFs to improve sensitivity. Moreover, extended response times are common, mainly due to the sluggish gas adsorption of ZIF-8, underscoring the ongoing need for additional exploration in this field. As highlighted earlier, the number of ZIF-8-coated Extrinsic Fabry-Perot Interferometer (EFPI) gas sensors is notably limited, offering a straightforward and cost-effective preparation process in contrast to other fiber optic interferometry systems.

Extrinsic Fabry-Perot Interferometric (EFPI) sensors with incorporated MOFs can be fabricated using two main approaches: top-down and bottom-up. The top-down method involves shaping bulk materials through processes like etching to create the desired cavity structure. Conversely, the bottom-up approach entails layer-by-layer assembly or growth from a substrate, offering precise control over composition and structure (this work). This is particularly useful for integrating MOFs with their distinct properties into the EFPI sensor design [46-50].

In this paper, we introduce a novel gas sensor applying a Fabry-Perot Interferometer with varied thicknesses of ZIF-8 coating on End-Faced Single-Mode Optical Fiber. This design offers improved sensitivity for selectively detecting small-molecule gases, exemplified by an ethanol sensor using ZIF-8 MOF within FP cavities. The innovative layer-by-layer technique was used to create impermeable ZIF-8 coatings on the fiber end, with enhanced thickness achieved through rinsing cycles and heat treatments. This advancement enabled ZIF-8 growth on the fiber, yielding coatings ranging from 800 nm to about 110 μm in thickness.

II. Experimental

A. Materials and end-faced coating

We prepared Zinc nitrate hexahydrate ($Zn(NO_3)_2 \cdot 6H_2O$) and 2-methylimidazole (2-mIm) from Sigma-Aldrich. A single-mode optical fiber (SMF-28, Corning Inc.) was used as the sensor fiber. The initial step involves stripping the polymer coatings from the single-mode fiber (SMF) using a stripper. The fiber is then cleaved using an optical fiber cleaver, resulting in a perfectly flat end face that is perpendicular to the direction of the fiber. After the cleaving process, the fiber is cleaned with alcohol and dried using N_2 gas.

The process involves coating ZIF-8 on the end facet of an optical fiber, followed by heating at 100°C for 50 minutes and subsequent etching in Buffer Oxide Etch (BOE) solution for around two hours, resulting in 5 cm of etched fiber. While heating the fiber before etching isn't always essential, it can improve the etching process by eliminating moisture that hinders chemical reactions and enhancing kinetic energy for more efficient and uniform etching. To apply a ZIF-8 thin film coating on the fiber end-face, a solution of $Zn(NO_3)2 \cdot 6H_2O$ (1.25 mM) and 2-mIm (5 mM) in methanol was prepared. The fiber tip was immersed in this solution at room temperature for 30 minutes. Afterward, the fiber tip was washed with fresh methanol to remove any unreacted zinc ions and 2-mIm and dried with N_2 gas (Fig.1). The fiber was then heated at 50°C for 10 min, and the ZIF-8 coating process was repeated as necessary to achieve the desired film thickness (cavity length).

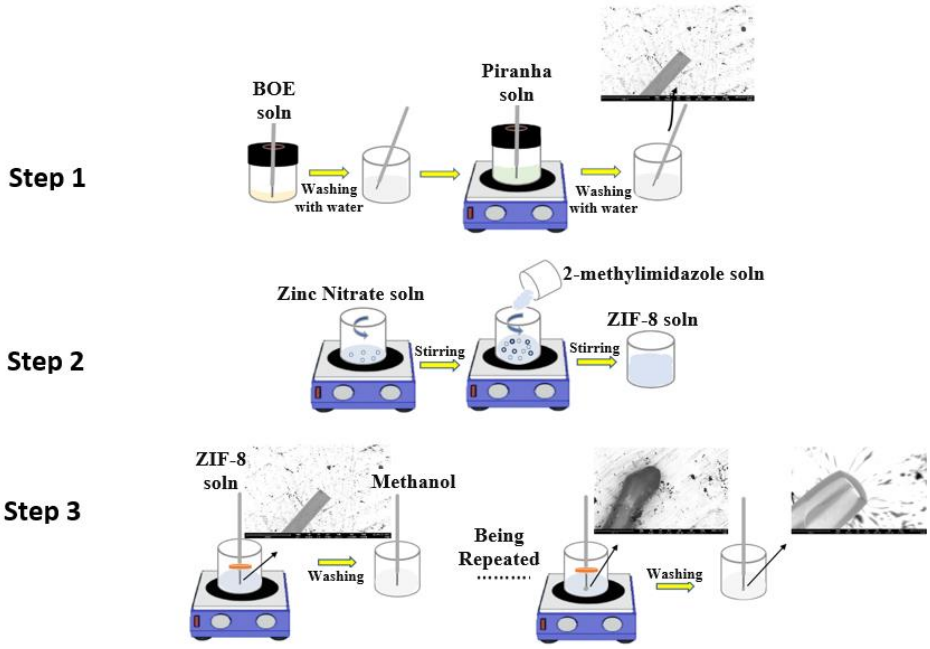

Fig. 1. Schematic illustration of the three main steps involved in creating ZIF-8 nanofilms on the end face of a single-mode optical fiber (SMF). The first step involves treating the end face of the optical fiber with a Buffer Oxide Etch (BOE) solution to etch it, followed by cleaning it with a piranha solution. The second step entails preparing a solution of ZIF-8, a crucial material for the coating process. In the final step, the end face is coated with the ZIF-8 solution through multiple cycles to achieve the desired thickness.

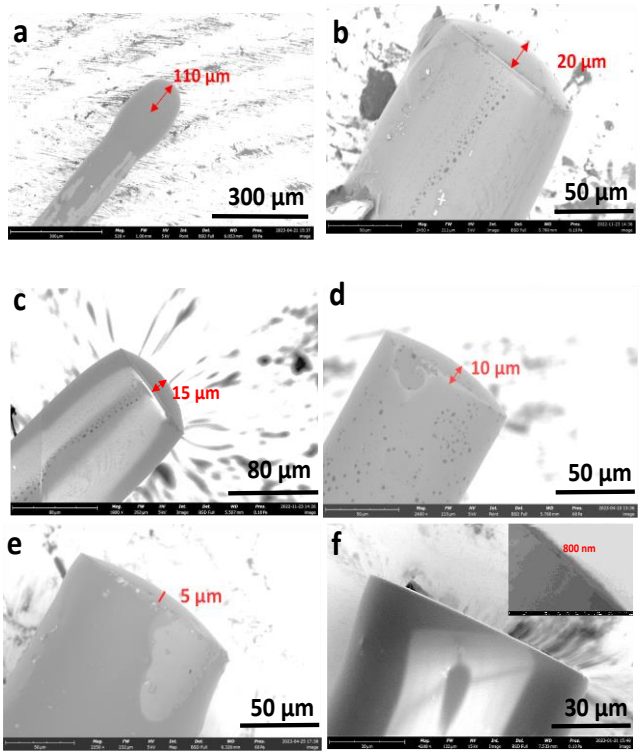

Fig. 2. The Representative Scanning Electron Microscope (SEM) images of ZIF-8 thin films of various thicknesses fabricated on the end-face of a single-mode optical fiber. The thicknesses depicted are (a) 110 µm. b) 20 µm. (c) 15 µm. (d) 10 µm. (e) 5 µm. (f) 800 nm.

Fig. 2 shows an SEM image of the fiber end-face with a ZIF-8 thin film coating. Film thickness was precisely controlled via coating cycle adjustments, leading to proportional growth with more cycles. Fig. 2(a-f) displays film thickness at different stages: 110 µm, 20 µm, 15 µm, 10 µm, 5 µm, and 800 nm. These ultra-thin nanofilms of ZIF-8 are defect-free and consistently structured with partial crystallinity, offering accessibility to small penetrants.

B. Coating ZIF-8 on one and both middle sides of the optic fiber

In the second part of our study, we attempted to grow ZIF-8 on both sides of the fiber, and in the subsequent part, we focused on growing it only on one side This approach offers the advantage of using fibers as heterostructure hybrids of MOFs and MOF-on-MOF hybrids.

We employed a straightforward step-by-step dip coating technique to investigate the formation of ZIF-8 on one and both middle sides of Single-Mode Fibers (SMF). This method is often described as relying on the attraction between positively and negatively charged polyelectrolytes in each layer deposited, which aids in understanding the technique. Rather than combining all the components and exposing them to specific conditions, we introduced each of them individually (see Fig. 3). Starting with an SMF, we gradually grew the MOF by immersing it into the $Zn(NO_3)2{\cdot}6H_2O$ (Zn^{2+}), washing it with a solvent, dipping it into a 2-methylimidazole (Hmim), and finally washing again. After each growth cycle, the surface was rinsed with methanol and allowed to dry. The one-sided coating of an optical fiber with ZIF-8 offers benefits such as the creation of hierarchical samples, enabling simultaneous measurement and reference/control on the uncoated side. This configuration allows for a specific sample's area definition, facilitating targeted gas sensing or analysis. Moreover, the versatility of the coating permits additional functionalization on the uncoated side, enhancing sensor performance and customization. Conversely, a both-sided coating of the optical fiber with ZIF-8 enhances gas sensing capabilities by increasing the surface area for improved detection of trace gases and low-concentration gas mixtures.

The step-by-step approach employed in this study ensures dense and uniform growth of metal-organic frameworks (MOFs) on the middle sides of the fiber, a challenging feat with conventional bulk synthesis methods. Unlike previous immersion methods, this approach yields continuous and uniform coatings, as illustrated in Fig. 4(a-b) with different ZIF-8 thicknesses. The final coating step involves applying approximately 10 µm thick ZIF-8 to one side of the fiber after surface treatment to enhance reactivity and smoothness. The fabrication of the fiber-optic Fabry-Perot (FP) nanocavity involves coating a ZIF-8 film on the end-face of a single-mode optical fiber (Fig. 2) for gas-sensing capabilities. Overall, both one-sided and both-sided ZIF-8 coatings on optical fibers hold promise for various applications, with the former offering hierarchical samples for simultaneous measurement and reference/control.

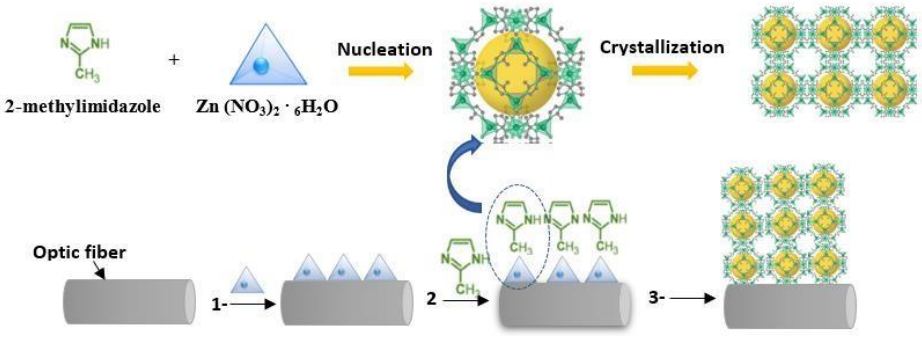

Fig. 3. The diagram depicts the sequential growth of ZIF-8. It forms by immersing alternately in $Zn(NO_3)2{\cdot}6H_2O$ and 2-mIm

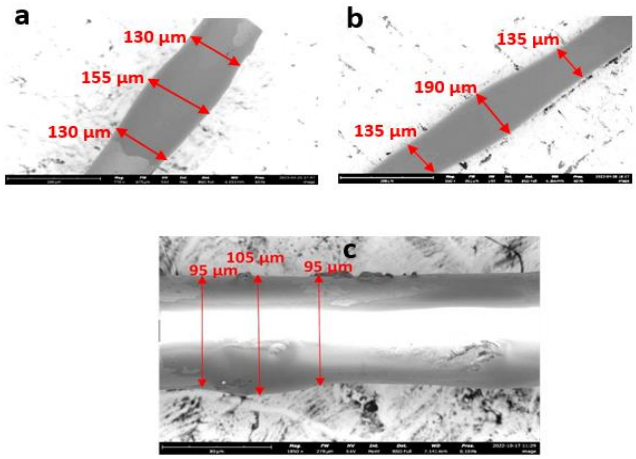

Fig. 4. SEM images of growing ZIF-8 on one and both sides of single-mode optic fibers. In one set of images, ZIF-8 is grown on both sides of the fiber, with a thickness of (a) 30 µm. (b) 65 µm. In another set of images, ZIF-8 is grown on only one side of the fiber, with a thickness of (c) 10 µm

C. Structural Analysis

The dual parameter sensing capability of the ZIF-8 coated optical fiber is enabled by functionalizing each side to selectively respond to different analytes. This feature allows for spatially resolved sensor arrays (based on the distributed sensing principle), which are useful in applications such as structural health monitoring, environmental monitoring, and security systems.

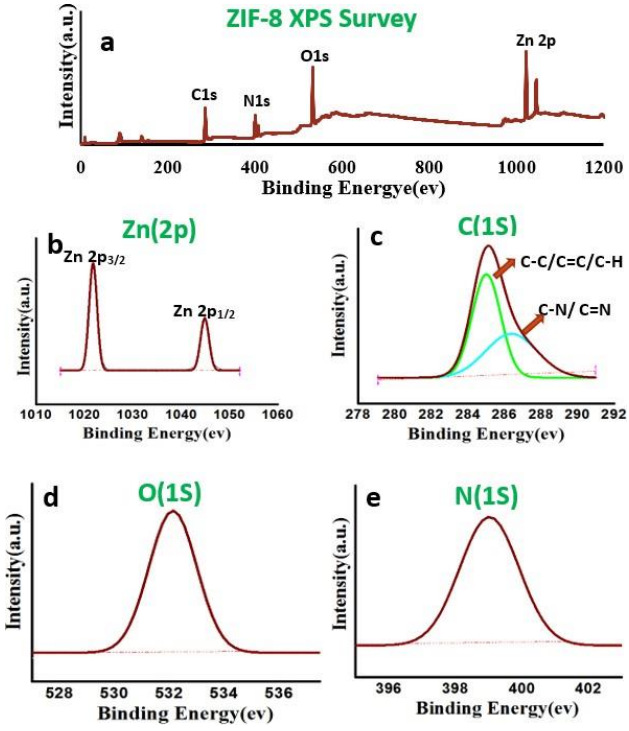

Fig. 5. X-ray Photoelectron Spectroscopy (XPS) spectra of ZIF-8 coated on the tip of the optical fiber. (a) A comprehensive survey spectrum of ZIF-8. (b) Zn 2p spectrum for ZIF-8. (c) C 1s spectrum for ZIF-8. (d) O 1s spectrum for ZIF-8. (e) N 1s XPS spectrum for ZIF-8.

The composition of the ZIF-8 coating was analyzed using X-ray Photoelectron Spectroscopy (XPS) across a wide range of binding energies (0-1100 eV), encompassing the Zn 2p, O 1s, N 1s, and C 1s regions (Fig. 5(a)). Specific regions were examined with higher pass energy and resolution. Fig. 5 shows the representative spectrum of a 4-cycle film. For enhanced zeolitic imidazolate framework (ZIF) signal, 4-cycle samples were used in XPS analysis. Detected features included zinc (coordinating metal), nitrogen, and carbon (from imidazole linker). XPS depth analysis is limited to the top 10 atomic layers, approximately 10 nm, depending on the photoelectron take-off angle. Smaller angles allow for more in-depth analysis. The binding energies of 1021.61 eV and 1044.88 eV were assigned to the Zn 2p3/2 and Zn 2p1/2 states, respectively (Fig. 5(b)). The separation between these two lines was measured at 23.27 eV, indicating the presence of Zn ions in the composites with a +2 state. The C(1s) spectrum revealed the presence of carbon materials, with a characteristic peak at approximately 285.0 eV attributed to C-C/C=C/C-H bonds, and another at 286.3 eV assigned to C-N/C=N bonds in 2-methylimidazole (2mIm). The O(1s) XPS spectrum of ZIF-8 exhibited a peak at 532.28 eV, corresponding to the bonding energy of O^{-2} ions, suggesting the presence of Zn-O bonds. In Fig. 5e, the sample displayed a single peak centered around 399.4 eV, representing the pyridinic nitrogen in 2mIm of ZIF-8. This indicates the presence of a single form of nitrogen within the sample [51-53].

III. Results and Discussion

A. Sensor fabrication and measurement principle

In the "Results and Discussion" section, we delve into the fabrication and measurement principle of the sensor. The sensor is constructed from an optical fiber (OF) with a ZIF-8 coating on its end face. This is visually represented in Fig. 6a, which provides a schematic diagram of the sensor, and in Fig. 6b, which shows an optical microscope image of the OF-ZIF-8 assembly.

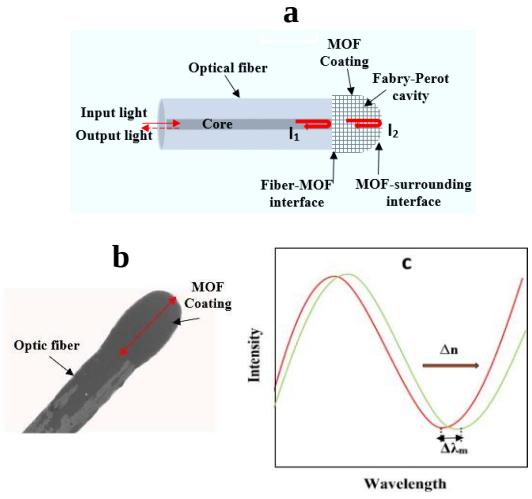

Fig. 6. The figure displays the design and structure of the OF-MOF sensor, along with interferogram shifts due to gas absorption. (a) Schematic of the sensor's design. (b) SEM image of the OF-MOF-based sensor's structure. (c) Original and shifted interferogram visualized, showing gas adsorption effects.

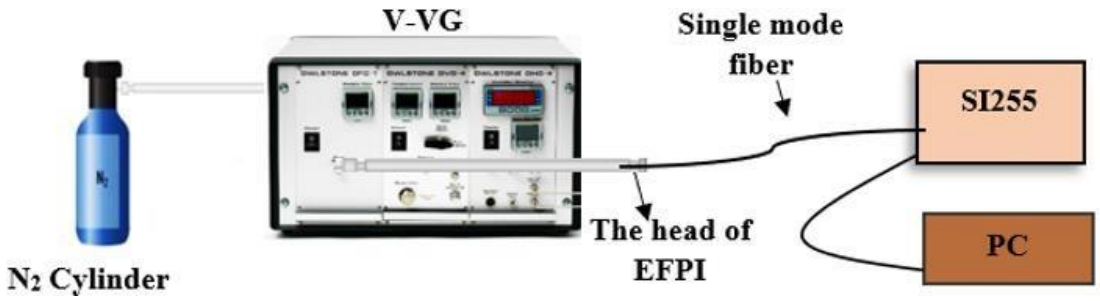

Fig. 7. Schematic diagram illustrating the sensor setup used for measuring gas sensing properties.

This setup forms a Fabry-Perot interferometer (FPI), with the interface between the optical fiber (OF) and the metal-organic framework (MOF) serving as one reflective surface, and the interface between the MOF and the surrounding medium acting as the other reflective surface. The MOF crystal functions as the medium within the Fabry-Perot cavity. Broadly speaking, a Fabry-Perot Interferometer (FPI) is a device composed of two parallel reflective surfaces. It is employed to measure physical parameters such as strain, pressure, or temperature to ascertain the desired physical parameter. As light travels through the core of the MOF coating material, a portion of it is reflected (I1) at the boundary between the optical fiber and the MOF coating material. The remaining light that continues through the MOF is then reflected (I2) at the boundary between the MOF coating material and its surroundings.

The interference signal, which arises from these two reflected light beams, can be calculated using Eq. 1 to determine its intensity as a function of wavelength (I).

$$I = I_1 + I_2 + 2\sqrt{I_1 I_2}\cos\left(\frac{4\pi nL}{\lambda} + \phi\right) \quad (1)$$

The equation incorporates the wavelength of the light used in the experiment (λ) and the initial phase difference between the two light beams (φ). The refractive index of the material inside the cavity, which comprises both the target substance under analysis and the host material, is denoted as 'n'. 'L' represents the physical length of the cavity (the thickness of the MOF coating material). When the phase difference between two partially reflected light beams satisfies a specific condition, an interference pattern of one or more minima emerges. In this pattern, the light waves periodically combine in a manner that minimizes the overall light intensity. The interference pattern is depicted in Fig. 6(c), and the specific wavelengths at which the valleys occur can be calculated using Eq. 2. Changes in the refractive index of the material inside the cavity affect the interference pattern, causing a shift in the wavelength of a particular valley in the pattern.

$$\frac{4\pi nL}{\lambda_m} = (2m+1)\pi \quad (2)$$

Each valley corresponds to a specific wavelength determined by an integer value (m), and the shift in wavelength ($\Delta\lambda_m$) is directly associated with the change in refractive index (Δn). This relationship is depicted in Fig. 6(c). By analyzing this pattern, we can determine the values of specific physical parameters through the observation of changes in refractive index, intensity, or wavelength.

$$\frac{\Delta\lambda_m}{\lambda_m} = \frac{\Delta n}{n} \quad (3)$$

Eq. 3 describes the relationship between the spectral changes in a material to the variations in its refractive index.

For MOFs, which have open pores, capturing molecules boosts the MOF's refractive index, altering its dielectric properties collectively. This occurs as all pore responses amalgamate. Monitoring this refractive index shift due to absorbed molecules lets us track and quantify their concentration within the MOF. The Fabry-Perot Interferometer (FPI), an optical interference method, precisely measures these refractive index changes by observing shifts in reflection spectra.

B. Gas sensing Setup

Fig. 7 depicts the system setup of the Optical Fiber-Metal Organic Framework (OF-MOF) used for measuring the adsorption of a specific chemical. The experimental setup includes Luna's HYPERION si255, an advanced optical sensing instrument capable of analyzing signals in high-speed, multipoint fiber optic sensing applications. This industrial-grade interrogator can perform both static and dynamic full-spectrum analysis, enabling reliable and accurate measurements from nearly 1000 sensors distributed across 16 parallel channels, each spanning a width of 160 nm. In this setup, the sensing element is a single-mode fiber (SMF). To create an effective sensing structure known as the Extrinsic Fabry-Perot Interferometer (EFPI), the fiber end face is coated with ZIF-8 of varying thicknesses, forming a thin film cavity. An Owlstone Vapor Generator (V-OVG) with a vertical oven is used to generate precise gas concentrations. The V-OVG is an Owlstone Vapor Generator designed with a vertically positioned oven to accommodate multiple permeation gas tubes.

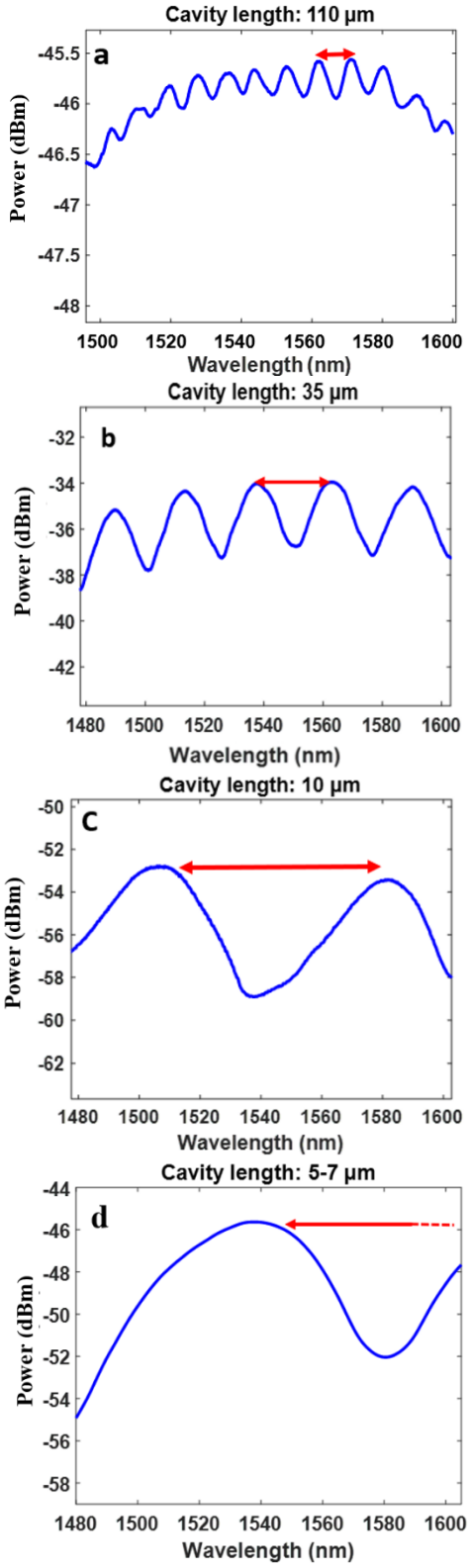

Fig. 8. Interferometric fringes of fabricated sensors with varying cavity lengths in air: (a) 110 µm, (b) 35 µm, (c) 10 µm, and (d) 5-7 µm. The red arrows indicate the free spectrum range, which is the distance between two consecutive peaks.

The results show interferograms from an Optical Fiber-Porous ZIF-8 micro-sensor with different ZIF-8 thicknesses: around 110 µm, 35 µm, 10 µm, and 6 µm (Fig. 8a-d). Upon initial examinationof these interference patterns, it is observed that the free spectral range (FSR) varies with the thickness of ZIF-8. Specifically, the FSR measures 8 nm, 25 nm, 88 nm, and 115 nm for the ZIF-8 thicknesses mentioned above, ordinary. These FSR measurements align with the thicknesses observed in the Scanning Electron Microscopy (SEM) images. They can also be calculated using the formula for the free spectral range (Eq.4)

$$FSR = \frac{c}{(2nL)} \quad (4)$$

where: c is the speed of light in a vacuum, n is the refractive index of the medium inside the cavity and L is the physical length of the cavity.

The correlation between FSR and ZIF-8 thickness offers insights into the Optical Fiber-Porous ZIF-8 micro-sensor. Thicker MOF coatings lead to reduced fringe visibility due to multiple-beam interference. Light waves interacting with different coating layers create constructive and destructive interference. Some light reflects at the coating-air interface, while some penetrates, reflecting at the core-coating interface, forming an interference pattern. For thin coatings or layers with an optimal thickness, the interference between the reflected waves results in constructive interference, leading to a strong and clear interference pattern with high fringe visibility. However, as the MOF coating becomes thicker, the phase difference between the multiple reflected waves changes, leading to destructive interference. This interference reduces the amplitude of the overall signal, resulting in lower fringe visibility. The decrease in fringe visibility affects the performance of the MOF-coated optical fiber in gas sensing applications, as it can impact the sensitivity and accuracy of the sensor. In practical applications, researchers aim to find an optimal coating thickness that maximizes the fringe visibility and sensor performance for the specific gas or analyte they want to detect. The uniformity of the interferogram is crucial as it signifies that the ZIF-8 material forms a consistent Fabry-Perot cavity, ensuring a well-defined and stable dimension for light transmission. The refractive index of the combined ZIF-8 and adsorbed molecules changes based on the number of molecules present when molecules are absorbed into the pores. The future advantage of porous ZIF-8 is its enhanced flexibility via modified silane groups on interior surfaces. This improves interactions with analyte molecules.

C. C_2H_6O Sensing measurement.

Our experiment utilized a Fabry-Perot interferometric (FPI) setup with a cavity length of 110 µm to measure the wavelength shift upon exposure to various concentrations of ethanol. In Fig. 9(a), the sensor's interferogram undergoes a three-step process. Initially, the spectra are collected for the as-prepared sensor (Before purge). In the second step, the reflection spectra are observed when the sensor cavity is filled with nitrogen, having a refractive index close to 1 (Nitrogen purge). The important parameter of sensitivity in this work is the wavelength shift, with a wavelength accuracy measurement of around 1 pm and a scan rate of 10 Hz.

.

This article has been accepted for publication in IEEE Sensors Journal. This is the author's version which has not been fully edited and content may change prior to final publication. Citation information: DOI 10.1109/JSEN.2024.3366872

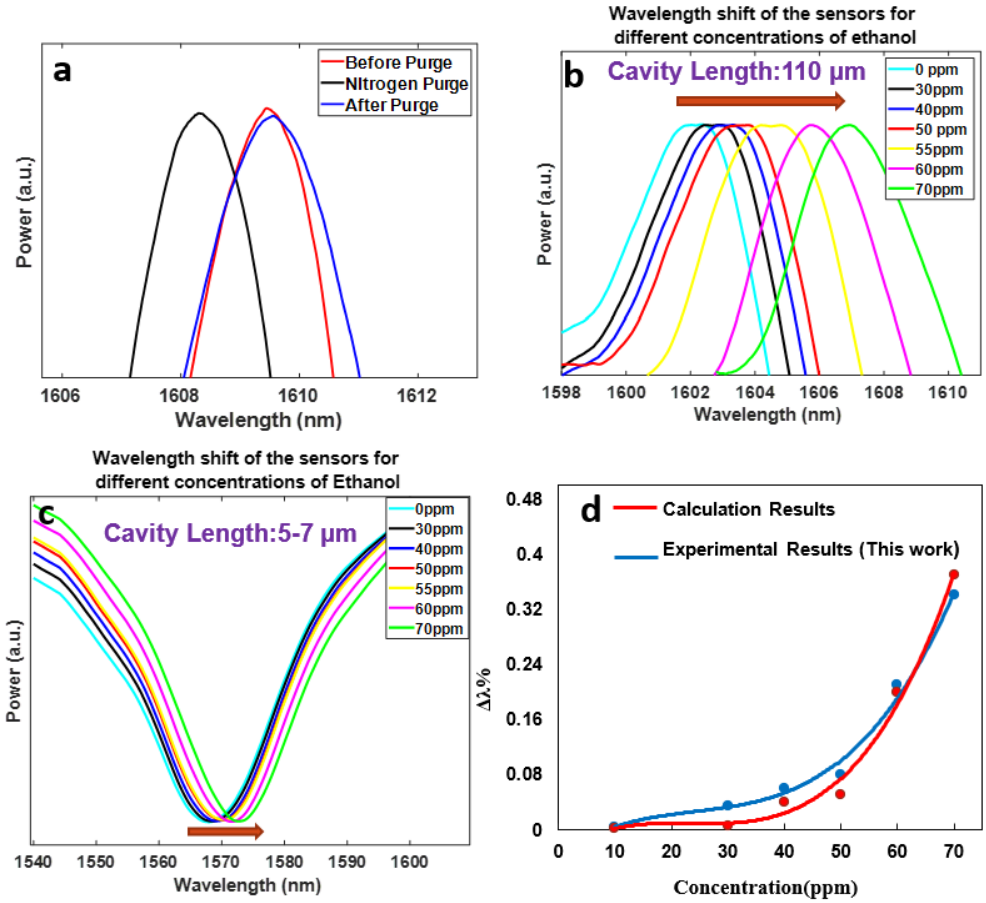

Fig. 9. The figure provides a comprehensive overview of the ZIF-8-FPI sensor's performance concerning interferogram shifts. (a) Interferogram shift of the ZIF-8 -FPI sensor when the cavity was filled with nitrogen. (b) Interferogram shift of the ZIF-8 -FPI sensor due to exposure to varying concentrations of ethanol for cavity lengths of 110 μm.(c) 5 μm. The red rows depict the direction of the wavelength shift resulting from ethanol absorption. (d) Δλ% change as a function of the ethanol concentration, compared with results from [54] (the solid curves in (d), are only used to guide the eye).

Following the nitrogen purge, a wavelength shift towards lower values occurs, attributed to a refractive index decrease resulting from the elimination of contaminants or water molecules within the ZIF-8 material pores, replaced by nitrogen. In the final step (After purge), the nitrogen is turned off, and the sensor is left in lab conditions for 30 minutes. The reflection spectra return to their initial position, indicating a reversal of the earlier shift. This reversion may be due to the high humidity level in the lab. Despite ZIF-8 being designed as a super-hydrophobic MOF, making it resistant to ambient water, the ambient moisture in the lab (approximately 16,000 ppm at room temperature and ~50% RH) could potentially replace nitrogen within the ZIF-8 pores when left at room temperature. Consequently, the reflection spectra return to their as-prepared state.

In the second phase of gas testing measurements, we used the setup depicted in Fig. 7 to record the sensor's interferogram in the atmosphere, both before and after exposure to ethanol. Interestingly, we observed that the sensor's interferogram returned to its original state after each measurement. This indicates that the ethanol adsorbed in the cavity was completely removed, leaving no impact on subsequent measurements. We successfully identified the change in wavelength (Δλ) by tracking the position of a specific fringe valley relative to its starting wavelength. The reflection spectra were measured when the sensor cavity contained ethanol of varying concentrations. As shown in Fig. 9(b) and 9(c), the sensor's fringes shifted toward longer wavelengths as the ethanol concentration increased. Specifically, for the Extrinsic Fabry-Perot Interferometer (EFPI) sensor with a ZIF-8 thickness of 110 μm, the wavelength position of the fringe valley at approximately 1602 nm in the air shifted to approximately 1602.55 nm, 1603.02 nm, 1603.38 nm, 1604.3 nm, 1605.5 nm, and 1606.8 nm for ethanol concentrations of 30 ppm, 40 ppm, 50 ppm, 55 ppm, 60 ppm, and 70 ppm, respectively. This method ensures reliable, repeatable, and highly sensitive measurements of gases.

The experiment was repeated using a sensor coated with ZIF-8 material at a thickness of 5 μm. Despite the challenge of obtaining precise measurements of wavelength changes due to the wide Free Spectral Range (FSR), the results aligned with those obtained for the sensor with a cavity length of 110 μm, as depicted in Fig. 9(c). The observed wavelength shift when ZIF-8 adsorbs nitrogen or ethanol is attributed to the interaction between the adsorbate molecules and the ZIF-8

framework. In ZIF-8, the adsorption of nitrogen or ethanol alters the local environment, impacting the material's refractive index and consequently causing a shift in the wavelength of light passing through it. In the case of nitrogen adsorption, the shift towards a lower wavelength, known as a blue shift, is likely due to the refractive index change caused by the presence of a minuscule amount of nitrogen within the pores of ZIF-8.

Very low volumetric concentrations of nitrogen have a lower refractive index compared to the MOF material, resulting in a decrease in the effective refractive index of the system to the lowest values measured. The unit cell of the ZIF-8 at STP contains a small amount of an ideal gas within 26 virtual unit cells, resulting in a total of 3.43 gas molecules. Nitrogen gas adsorption is slight, with a concentration ratio of 1.324 compared to the empty space. Ethanol adsorption in ZIF-8 leads to a significant increase in refractive index due to a concentration ratio of 2408.4, causing a red-shift in light wavelength. Ethanol becomes the main adsorbate at room temperature, influencing RI calculations, but the exact wavelength shift depends on factors like concentration and experimental conditions. Equation 3 can be used to calculate RI change [54]. The results obtained, as shown in Fig. 9(d), align closely with the findings reported in our previous publication. This suggests that the wavelength shift resulting from the adsorption of ethanol, within the concentration range of 30 ppm to 70 ppm, is consistent with previously reported data, thereby confirming the high accuracy of our calculations.

The concluding part of our analysis concentrated on the response and recovery times of ZIF-8- FPI-based sensors with cavity lengths of 110 μm and 10 μm. These sensors were subjected to 70 ppm ethanol at standard temperature and pressure (STP) conditions. The response time, denoting 90% change in the final response, and recovery time, indicating the time to reach 10% of the initial value, were investigated. At room temperature, the 110 μm cavity sensor displayed response and recovery times of roughly 1 minute and 4 minutes, respectively. Conversely, the 10 μm cavity sensor exhibited quicker response and recovery times, approximately 17 seconds and 50 seconds, under identical conditions. Although the recovery time surpassed the response time, needing around 5 minutes and 1 minute to revert to the original spectrum after air exposure, both times involve two phases: gas molecule diffusion into the sensor’s surface and their absorption onto the surface. Nanostructure gaps serve as channels for gas diffusion, intimately linking response and recovery times to absorption and desorption processes.
Unlike previous studies (as reported in Table 1.) that focused on employing ZIF-8 in conjunction with various substances like Oleylamine (OLA), Cobalt (Co), and graphene oxide (GO) to detect gases such as carbon dioxide and ethanol, this research exclusively explores ZIF-8 coating as EFPI gas sensors with high sensitivity and low response time (17 s) compare with previous Optical fiber ZIF-8 gas sensors. Moreover, few publications have employed ZIF-8 coating on the end face of optical fiber as EFPI gas sensors (relatively new research), demonstrating heightened sensitivity and relatively swift response times when compared to alternative optical fiber gas sensor methodologies.

The systematic investigation of ZIF-8 at different thicknesses provides comprehensive insights into their impact on sensor performance, allowing for optimized sensor design and tailored applications. Overall, this study significantly contributes to advancing MOF-based optical fiber sensors, particularly in the context of EFPI sensors, opening avenues for enhanced sensitivity and selectivity in gas detection applications and paving the way for further advancements in the field.

IV. Discussion

The Extrinsic Fabry-Perot Interferometer (EFPI) optical fiber sensor is a device that utilizes the principles of interferometry. It consists of a cleaved optical fiber with a cavity formed between two reflective surfaces. When light is transmitted through the optical fiber, a portion of it is reflected at each of the reflective surfaces. The reflected light waves interfere with each other, creating an interference pattern that is highly sensitive to changes in the cavity's length.

To detect ethanol, the EFPI optical fiber sensor is coated with a layer of ZIF-8 (Zeolitic Imidazolate Framework-8), which is a metal-organic framework known for its porous structure. This porous structure allows ZIF-8 to adsorb gas molecules, such as ethanol. Upon encountering an environment with ethanol vapor, the ZIF-8-coated sensor absorbs ethanol molecules into the pores of the ZIF-8 material. As these molecules are adsorbed, the effective length of the EFPI cavity changes. This change in cavity length leads to a shift in the interference pattern of the reflected light. The interference pattern is sensitive to changes in the cavity length, and as ethanol is adsorbed into the ZIF-8 coating, the wavelength of light that maximizes constructive interference in the cavity changes. This shift in wavelength can be precisely measured by the sensor, providing a means to detect the presence and concentration of ethanol.

The response time and recovery time of the sensor are influenced by the thickness of the ZIF-8 coating. A thinner ZIF-8 coating generally results in faster response and recovery times. This is because a thinner coating allows ethanol molecules to quickly penetrate the coating and interact with the porous material. In terms of the response time, a thinner ZIF-8 coating shortens the diffusion pathways for ethanol molecules, enabling the sensor to detect changes in ethanol concentration more rapidly. For the recovery time, a thinner coating facilitates the release of adsorbed ethanol molecules more quickly, allowing the sensor to return to its initial state faster [11, 19, 21, 25]. However, it's important to find the right balance in coating thickness. An excessively thin coating may sacrifice sensitivity, while an excessively thick one might slow down the sensor's response and recovery times. The optimal thickness depends on the specific application and the desired trade-off between sensitivity and speed of response and recovery.

This article has been accepted for publication in IEEE Sensors Journal. This is the author's version which has not been fully edited and content may change prior to final publication. Citation information: DOI 10.1109/JSEN.2024.3366872

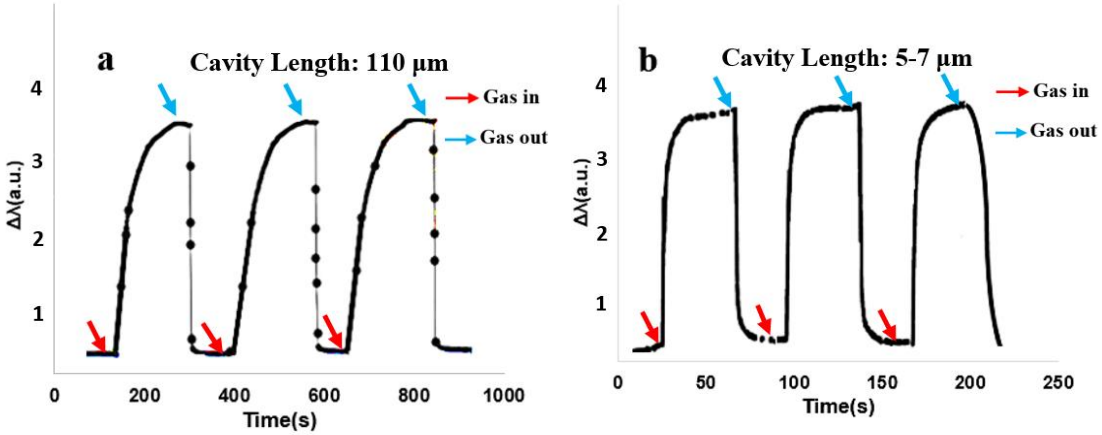

Fig. 10. Observation of the time-dependent behavior of Fabry-Perot Interferometer (FPI) sensors coated with ZIF-8 under the influence of 50 ppm ethanol gas at room temperature. The response and recovery times were measured for two different cavity lengths: (a) 110 µm. (b) 5-7 µm.

Table 1. Comparison of the performance of ZIF-8 film-based fiber-optic gas sensor across the different evaluation techniques

Sensor type	Coated Materials	Detection Gas	T (^{0}C)	Data evaluation technique	Coated Thickness	Conc. Range	Response Time/ Recovery Time	Ref
Optical Fiber and Surface Acoustic Wave-Based Sensors	Oleylamine (OLA)/Cobalt (Co)/ZIF-8	Carbon dioxide	RT	Δ Transmission	200 nm	0-100 Vol%	~5 to 10 min/~5 to 10 min	[45]
Optical Microfiber Interferometric	ZIF-8/GO	EtOH	RT	Δ λ (3.8 pm/ppm)	138 nm	5.26 to 6850 ppm	11.8 s/10.1s	[44]
Internal Fabry–Perot interferometer (IFPI)	ZIF-8/PDMS	Methan	RT	$\Delta I/I_0$	120 µm	0-100 Vol %	250–500 s/ –	[43]
Long-period fiber grating (LPFG)	ZIF-8	Methan	RT	Δ Transmission	100 nm–400 nm	1454 to 27900 ppm	~3 min/5 min	[26]
Long-period fiber grating (LPFG)	ZIF-8	EtOH	RT	Δ Bandwidth (0.018 ± 0.0015 nm/ppm)	250 nm	5.56 to 666 ppm	–	[42]
Optical Fiber Waveguide Platform	ZIF-8, Cobalt (Co)/ZIF-8	Carbon dioxide	RT	ΔRI	200 nm–530 nm	0-100 Vol %	9s/14s 24s/84s	[41]
Fiber Mach–Zehnder interferometer (MZI) with a pair of LPEGs	ZIF-8	EtOH	RT	Δλ (1.33 pm/ppm)	300 nm	9.8 to 540 ppm	-	[55]
Internal Fabry–Perot interferometer (EFPI)	ZIF-8	EtOH	RT	Δ λ (~ 0.1 nm/ppm)	800 nm–110 µm	5 to 70 ppm	17 s/37 s	This work

V. CONCLUSION

In our recent study, we created a fiber-optic Fabry-Pérot microcavity for gas sensing purposes by applying a ZIF-8 film to the end of a single-mode optical fiber. This was achieved through layer-by-layer synthesis and pre-post-treatment methods using SEM and XPS methods. The gas sensor based on this setup exhibited wavelength shifts in its fringes as ethanol concentration increased, with the shift being related to the thickness of the ZIF-8 coating. This correlation was supported by SEM images and mathematical calculations.

Both experimental and calculated data demonstrated a strong link between wavelength shifts and ethanol concentration. Moreover, reducing the thickness of the MOF coating led to a remarkable 400% decrease in response time and 500% decrease in recovery time. In summary, our research centered on detecting changes in the Fabry-Pérot Interferometric optical path due to varying levels of volatile organic compounds, enabling wavelength shifts that can be measured for gas sensing.

Data Availability

Data will be made available on request.

Acknowledgments

This work was supported by the Army Research Laboratory and was accomplished under Cooperative Agreement Number W911NF-21-2-0274. The views and conclusions contained in this document are those of the authors and should not be interpreted as representing the official policies, either expressed or implied, of the Army Research Office or the U.S. Government. The U.S. Government is authorized to reproduce and distribute reprints for Government purposes notwithstanding any copyright notation herein.

Appendix A. Supporting information.

Supplementary material related to this article is available.

References

[1] D. Chaudhary, S. Nayse, and L. Waghmare, "Application of wireless sensor networks for greenhouse parameter control in precision agriculture," *International Journal of Wireless & Mobile Networks (IJWMN)*, vol. 3, no. 1, pp. 140-149, 2011.

[2] M. Folke, L. Cernerud, M. Ekström, and B. Hök, "Critical review of non-invasive respiratory monitoring in medical care," *Medical and Biological Engineering and Computing*, vol. 41, pp. 377-383, 2003.

[3] H.-T. Kim, W. Hwang, Y. Liu, and M. Yu, "Ultracompact gas sensor with metal-organic-framework-based differential fiber-optic Fabry-Perot nanocavities," *Optics Express*, vol. 28, no. 20, pp. 29937-29947, 2020.

[4] A. Nikfarjam, and N. Salehifar, "Improvement in gas-sensing properties of TiO_2 nanofiber sensor by UV irradiation." *Sensors and Actuators B: Chemical,vol.* 211, pp. 146-156, 2015.

[5] J. Mulrooney, J. Clifford, C. Fitzpatrick, and E. Lewis, "Detection of carbon dioxide emissions from a diesel engine using a mid-infrared optical fibre based sensor," *Sensors and Actuators A: Physical*, vol. 136, no. 1, pp. 104-110, 2007.

[6] S. Neethirajan, D. Jayas, and S. Sadistap, "Carbon dioxide (CO_2) sensors for the agri-food industry—a review," *Food and Bioprocess Technology*, vol. 2, pp. 115-121, 2009.

[7] T. J. Pfeiffer, S. T. Summerfelt, and B. J. Watten, "Comparative performance of CO2 measuring methods: Marine aquaculture recirculation system application," *Aquacultural engineering*, vol. 44, no. 1, pp. 1-9, 2011.

[8] M. Hosseini, S. Zeinali, and M. Sheikhi, "Fabrication of capacitive sensor based on Cu-BTC (MOF-199) nanoporous film for detection of ethanol and methanol vapors," *Sensors and Actuators B: Chemical*, vol. 230, pp. 9-16, 2016.

[9] J. E. Ellis, S. E. Crawford, and K.-J. Kim, "Metal–organic framework thin films as versatile chemical sensing materials," *Materials Advances*, vol. 2, no. 19, pp. 6169-6196, 2021.

[10] Z.-Z. Lu, R. Zhang, Y.-Z. Li, Z.-J. Guo, and H.-G. Zheng, "Solvatochromic behavior of a nanotubular metal− organic framework for sensing small molecules," *Journal of the American Chemical Society*, vol. 133, no. 12, pp. 4172-4174, 2011.

[11] C. Zhu, R. E. Gerald, and J. Huang, "Metal-organic framework materials coupled to optical fibers for chemical sensing: A review," *IEEE sensors journal*, vol. 21, no. 18, pp. 19647-19661, 2021.

[12] Zou, Xiaoqin, et al. "Synthesis of a metal–organic framework film by direct conversion technique for VOCs sensing." *Dalton Transactions*, no. 16, pp. 3009-3013, 2009.

[13] L.-G. Qiu, Z.-Q. Li, Y. Wu, W. Wang, T. Xu, and X. Jiang, "Facile synthesis of nanocrystals of a microporous metal–organic framework by an ultrasonic method and selective sensing of organoamines," *Chemical communications*, no. 31, pp. 3642-3644, 2008.

[14] V. Mihalef *et al.*, "Patient-specific modelling of whole heart anatomy, dynamics and haemodynamics from four-dimensional cardiac CT images," *Interface Focus*, vol. 1, no. 3, pp. 286-296, 2011.

[15] S. Khan, S. Le Calvé, and D. Newport, "A review of optical interferometry techniques for VOC detection," *Sensors and Actuators A: Physical*, vol. 302, p. 111782, 2020.

[16] G. Lu and J. T. Hupp, "Metal− organic frameworks as sensors: a ZIF-8 based Fabry− Pérot device as a selective sensor for chemical vapors and gases," *Journal of the American Chemical Society*, vol. 132, no. 23, pp. 7832-7833, 2010.

[17] L. E. Kreno, J. T. Hupp, and R. P. Van Duyne, "Metal− organic framework thin film for enhanced localized surface plasmon resonance gas sensing," *Analytical chemistry*, vol. 82, no. 19, pp. 8042-8046, 2010.

[18] Hodgkinson, Jane, and Ralph P. Tatam. "Optical gas sensing: a review," *Measurement science and technology*, vol. 24, no.1, pp. 012004, 2012.

[19] Y. Du, S. Jothibasu, Y. Zhuang, C. Zhu, and J. Huang, "Rayleigh backscattering based macro bending single-mode fiber for distributed refractive index sensing," *Sensors and Actuators B: Chemical*, vol. 248, pp. 346-350, 2017.

[20] X. Wei, T. Wei, H. Xiao, and Y. Lin, "Nano-structured Pd-long period fiber gratings integrated optical sensor for hydrogen detection," *Sensors and Actuators B: Chemical*, vol. 134, no. 2, pp. 687-693, 2008.

[21] C. Zhu, Y. Zhuang, B. Zhang, R. Muhammad, P. P. Wang, and J. Huang, "A miniaturized optical fiber tip high-temperature sensor based on concave-shaped Fabry–Perot cavity," *IEEE Photonics Technology Letters*, vol. 31, no. 1, pp. 35-38, 2018.

[22] J. Chen, B. Liu, and H. Zhang, "Review of fiber Bragg grating sensor technology," *Frontiers of Optoelectronics in China*, vol. 4, pp. 204-212, 2011.

[23] V. M. Passaro, A. Cuccovillo, L. Vaiani, M. De Carlo, and C. E. Campanella, "Gyroscope technology and applications: A review in the industrial perspective," *Sensors*, vol. 17, no. 10, p. 2284, 2017.

[24] B. H. Lee *et al.*, "Interferometric fiber optic sensors," *sensors*, vol. 12, no. 3, pp. 2467-2486, 2012.

[25] C. Zhu, J. A. Perman, R. E. Gerald, S. Ma, and J. Huang, "Chemical detection using a metal–organic framework single crystal coupled to an optical fiber," *ACS applied materials & interfaces*, vol. 11, no. 4, pp. 4393-4398, 2019.

[26] J. Hromadka, B. Tokay, S. James, R. P. Tatam, and S. Korposh, "Optical fibre long-period grating gas sensor modified with metal-organic framework thin films," *Sensors and Actuators B: Chemical*, vol. 221, pp. 891-899, 2015.

[27] J. Tao *et al.*, "Hybrid photonic cavity with metal-organic framework coatings for the ultra-sensitive detection of volatile organic compounds with high immunity to humidity," *Scientific reports*, vol. 7, no. 1, p. 41640, 2017.

[28] R. Zhang *et al.*, "Metal–Organic Framework Crystal-Assembled Optical Sensors for Chemical Vapors: Effects of Crystal Sizes and Missing-Linker Defects on Sensing Performances," *ACS Applied Materials & interfaces*, vol. 11, no. 23, pp. 21010-21017, 2019.

[29] M. P. Suh, H. J. Park, T. K. Prasad, and D.-W. Lim, "Hydrogen storage in metal–organic frameworks," *Chemical reviews*, vol. 112, no. 2, pp. 782-835, 2012.

[30] J.-R. Li, J. Sculley, and H.-C. Zhou, "Metal–organic frameworks for separations," *Chemical reviews*, vol. 112, no. 2, pp. 869-932, 2012.

[31] J.-R. Li, R. J. Kuppler, and H.-C. Zhou, "Selective gas adsorption and separation in metal–organic frameworks," *Chemical Society Reviews*, vol. 38, no. 5, pp. 1477-1504, 2009.

[32] M. Yoon, R. Srirambalaji, and K. Kim, "Homochiral metal–organic frameworks for asymmetric heterogeneous catalysis," *Chemical reviews*, vol. 112, no. 2, pp. 1196-1231, 2012.

[33] L. E. Kreno, K. Leong, O. K. Farha, M. Allendorf, R. P. Van Duyne, and J. T. Hupp, "Metal–organic framework materials as chemical sensors," *Chemical reviews*, vol. 112, no. 2, pp. 1105-1125, 2012.

[34] D. Ma *et al.*, "A dual functional MOF as a luminescent sensor for quantitatively detecting the concentration of nitrobenzene and temperature," *Chemical Communications*, vol. 49, no. 79, pp. 8964-8966, 2013.

[35] X. Chong *et al.*, "Near-infrared absorption gas sensing with metal-organic framework on optical fibers," *Sensors and Actuators B: Chemical*, vol. 232, pp. 43-51, 2016.

[36] Lu, Lidan, Lianqing Zhu, Guixian Zhu, Mingli Dong, and Zhoumo Zeng. "ZIF-8/lipase coated tapered optical fiber biosensor for the

detection of triacylglycerides." *IEEE Sensors Journal*, vol. 20, no. 23, pp. 14173-14180, 2020.

[37] M. Nazari *et al.*, "UiO-66 MOF end-face-coated optical fiber in aqueous contaminant detection," *Optics Letters*, vol. 41, no. 8, pp. 1696-1699, 2016.

[38] K. Zhan, Z. Wang, Y. Zhu, J. Yan, and Y. Chen, "Nano-Porous UIO-66-NH_2/TiO_2 Bragg Reflector for Low Concentration HCl Gas Sensing," *IEEE Sensors Journal*, vol. 21, no. 15, pp. 16469-16474, 2021.

[39] K. S. Park *et al.*, "Exceptional chemical and thermal stability of zeolitic imidazolate frameworks," *Proceedings of the National Academy of Sciences*, vol. 103, no. 27, pp. 10186-10191, 2006.

[40] A. Demessence *et al.*, "Adsorption properties in high optical quality nano ZIF-8 thin films with tunable thickness," *Journal of Materials Chemistry*, vol. 20, no. 36, pp. 7676-7681, 2010.

[41] K. J. Kim, P. Lu, J. T. Culp and P. R. Ohodnicki, "Metal–organic framework thin film coated optical fiber sensors: a novel waveguide-based chemical sensing platform," *ACS Sensors*, vol. 3, no. 2, pp. 386-394, 2018.

[42] J. Hromadka, B. Tokay, R. Correia, S.R. Morgan, and S. Korposh, "Highly sensitive volatile organic compounds vapor measurements using a long period grating optical fiber sensor coated with metal-organic framework ZIF-8," *Sensors and actuators B: chemical*, vol. 260, pp. 685-692, 2018.

[43] R. Cao, H. Ding, K. J. Kim, Z. Peng, J. Wu, J. T. Culp, P. R. Ohodnicki, E. Beckman, and K. P. Chen, "Metal-organic framework functionalized polymer coating for fiber optical methane sensors," *Sensors and Actuators B: Chemical*, vol. 324, pp. 128627, 2020.

[44] Y. Huang, W. Lin, T. Huang, Z. Li, Z. Zhang, R. Xiao, X. Yang, S. Lian, J. Pan, J. Ma, and W. Wang, "Ultrafast response optical microfiber interferometric VOC sensor based on evanescent field interaction with ZIF-8/graphene oxide nanocoating," *Advanced Optical Materials*, vol. 10, no. 3, pp. 2101561, 2022.

[45] K. J. Kim, J. T. Culp, P. R. Ohodnicki, P. C. Cvetic, S. Sanguinito, A. L. Goodman, and H. T. Kwon, "Alkylamine-integrated metal–organic framework-based waveguide sensors for efficient detection of carbon dioxide from humid gas streams," *ACS Applied Materials & interfaces*, vol. 11, no. 36, pp. 33489-33496, 2019.

[46] K. Babaei Gavan, J. H. Rector, K. Heeck, D. Chavan, G. Gruca, T. H. Oosterkamp, and D. Iannuzzi. "Top-down approach to fiber-top cantilevers", *Optics Letters*, vol. 36, no. 15, pp. 2898–2900, 2011.

[47] D. Iannuzzi, S. Deladi, V. J. Gadgil, R. G. P. Sanders, H. Schreuders, and M. C. Elwenspoek. "Monolithic fiber-top sensor for critical environments and standard applications". *Applied Physics Letters*, vol. 88, no. 5, pp. 053501, 2006.

[48] B. D. Gupta, A. Pathak, and A. M. Shrivastav, "Optical Biomedical Diagnostics Using Lab-on-Fiber Technology: A Review, " *Photonics*, vol. 9, no. 2, pp. 86, 2022.

[49] A. Paul, I. K. Banga, S. Muthukumar, and S. Prasad, "Engineering the ZIF-8 pore for electrochemical sensor applications─ a mini review," *ACS omega*, vol. 7, no. 31, pp. 26993-27003, 2022.

[50] N. C. Keppler, K. D. J. Hindricks, and P. Behrens, "Large refractive index changes in ZIF-8 thin films of optical quality," *RSC advances*, vol. 12, no. 10, pp. 5807-5815, 2022.

[51] J. Liu *et al.*, "NiO-PTA supported on ZIF-8 as a highly effective catalyst for hydrocracking of Jatropha oil," *Scientific reports*, vol. 6, no. 1, pp. 23667, 2016.

[52] S. Luanwuthi, A. Krittayavathananon, P. Srimuk, and M. Sawangphruk, "In situ synthesis of permselective zeolitic imidazolate framework-8/graphene oxide composites: rotating disk electrode and Langmuir adsorption isotherm," *RSC Advances*, vol. 5, no. 58, pp. 46617-46623, 2015.

[53] M. Hayashi, D. T. Lee, M. D. de Mello, J. A. Boscoboinik, and M. Tsapatsis, "ZIF-8 membrane permselectivity modification by manganese (II) acetylacetonate vapor treatment," *Angewandte Chemie International Edition*, vol. 60, no. 17, pp. 9316-9320, 2021.

[54] N. Salehifar, P. Holtmann, A. P. Hungund, H. S. Dinani, R. E. Gerald, and J. Huang, "Calculations of adsorption-dependent refractive indices of metal-organic frameworks for gas sensing applications," *Optics Express*, vol. 31, no. 5, pp. 7947-7965, 2023.

[55] J. Wu, W. Zhang, Y. Wang, B. Li, T. Hao, Y. Zheng, L. Jiang, K. Chen, and K. S. Chiang, "Nanoscale light–matter interactions in metal–organic frameworks cladding optical fibers," *Nanoscale*, vol. 12, no. 18, pp. 9991-10000, 2023.